SAND2007-3529C

COMPUTATIONAL COMBUSTION 2007, ECCOMAS Thematic Conference
D. Roekaerts, P. Coelho, B.J. Boersma, K. Claramunt (Eds.)
18-20 July 2007, Delft, The Netherlands

DIRECT NUMERICAL SIMULATION OF SOOT FORMATION IN A THREE-DIMENSIONAL NONPREMIXED ETHYLENE JET FLAME

David O. Lignell[*,†] **and Jacqueline H. Chen**[†]

[*]The University of Utah, Department of Chemical Engineering
155 S. 1452 E. 380 INSCC, Salt Lake City, UT 84112
e-mail: david@crsim.utah.edu, web page: http://www.inscc.utah.edu/∼david,

[†]Reacting Flow Research Department, Combustion Research Facility, Sandia National Laboratories
7011 East Avenue, Livermore CA 94551-9051
e-mail: jhchen@sandia.gov

Key words: DNS, Soot, Nonpremixed, Ethylene, Jet, CMC

Abstract. *Three-dimensional direct numerical simulation with soot formation is presented for the first time. A temporally evolving, planar, nonpremixed ethylene jet flame was simulated with a validated, 19-species reduced mechanism. A 4-step, 3-moment, semi-empirical soot model was employed. Previous two-dimensional simulations have shown the importance of multi-dimensional flame dynamical effects on soot concentration. It was shown that flame curvature strongly impacts the diffusive motion of the flame relative to soot (which is essentially convected with the flow), resulting in soot being differentially transported toward or away from the flame zone. The proximity of the soot to the flame directly influences soot reactivity and radiative properties. Here, the analysis is extended to three dimensions with mean shear, and show that similar flame dynamic effects are important. Soot modelling in turbulent flames is a challenge due to the complexity of soot formation and transport processes, and the lack of detailed experimental soot-flame-flow structural data. The present DNS provides the first step towards providing such data.*

1 INTRODUCTION

Soot formation in turbulent hydrocarbon combustion is of great practical importance. Soot emission is a known health hazard, and its presence indicates reduced combustion efficiency. Soot formation is responsible for the bulk of flame luminosity and radiative heat transfer. For these reasons, and others, soot formation in laminar and turbulent flames is the subject of intense research. Soot formation in flames, particularly turbulent flames, is a complex process involving a rich set of physical phenomena that make experimental and computational research challenging. Some of the difficulties are

- Soot formation chemistry involves a large number of increasingly high molecular weight species: notably formation and growth involving PAH.
- Soot exists as a particle phase with a continuous size distribution, which must be accounted for in conjunction with the gas chemistry.
- Flames with substantial soot concentrations can be optically thick with respect to radiative heat transfer.
- Transport of soot occurs primarily via thermophoresis, and, as a particle phase, soot is transported differentially to gaseous species.
- The timescales of soot formation are longer than typical combustion timescales, resulting in overlap of soot chemistry and large-scale flow features.

Many detailed analyses of soot-flame interactions have been performed that characterize soot concentration, temperature, particle distribution, and relevant chemical flow fields. However, these detailed experimental and computational studies have been limited mainly to well-characterized, canonical configurations in laminar, steady (and some unsteady) flows.[1,2] Experimental studies of turbulent sooting flames are limited to providing statistical quantities (e.g. means of soot volume fraction and number density), and cannot resolve detailed flame-soot-flow structure interactions due to the optical thickness of the flames and the thin structures of the soot layers. Large scale turbulent simulations using RANS or LES approaches use subgrid models adapted to soot formation,[3,4] but detailed soot-flame structure data in turbulent environments is not available for model development and validation.

Direct numerical simulation (DNS) resolves all flow and chemical scales, and is currently the only feasible method that can provide details of the full spatial and temporal reacting flow field. We have extended three-dimensional reacting DNS to combustion with soot formation for the first time. The goal of the DNS simulations is twofold: (1) to provide detailed data that can be used to develop and validate subgrid chemistry models for large-scale practical applications, and (2), to gain fundamental physical insight into soot-flame-flow interactions. As discussed in more detail below, the DNS configuration consists of a temporally-evolving, non-premixed ethylene jet flame with a validated 19-species reduced ethylene mechanism, and a 4-step, 3-moment, semi-empirical soot model.

We recently performed two-dimensional simulations of soot formation in decaying turbulence[5] to study the effects of unsteady, multi-dimensional flame dynamics on soot formation and transport processes. There, it is shown that differential diffusion between the soot and the flame determines the proximity of the soot to the flame, and hence the temperature and composition characteristics that the soot. These, in turn, directly influence rates of soot reaction(hence concentration) and radiation. Soot transport occurs mainly via convection and thermophoresis, while flame surface motion occurs via diffusion and convection. The relative motion between soot and the flame zone was quantified by

examining the flame motion relative to convection, termed the *flame displacement velocity*, v_ξ. Since soot is mainly convected with the flow, the sign of v_ξ determines whether soot is convected into, or away from the high temperature, oxidizing flame. This velocity derives from two terms: a flame curvature term, and diffusion resolved in the direction normal to the flame surface, referred to as the "normal diffusion term". It was found that both terms were important, and the former is inherently multi-dimensional. It was further found that a substantial portion of the flow experienced regions of both sign of v_ξ. In regions where the center of flame curvature was in the fuel stream, the flame motion was shifted in the direction of the fuel stream (soot convected towards the flame, giving higher soot concentrations), and vice-versa. These flame dynamic effects are not directly included in RANS and LES simulations involving soot formation, so this quantification is important. Here we extend the previous analysis to a three-dimensional configuration. We examine the flame displacement velocity and its budget, as well as the role of the thermophoretic velocity.

2 NUMERICAL IMPLEMENTATION

The DNS simulation was performed using S3D, developed at Sandia National Laboratories. S3D explicitly integrates the three-dimensional reacting, compressible Navier Stokes equations in time using a 4^{th} order, 6-stage Runge-Kutta algorithm.[6] Spatial discretization on a uniform, Cartesian grid is performed using 8^{th} order central difference approximations to derivatives. A 10^{th} order spatial filter is applied at each timestep to remove high wavenumber content and reduce aliasing errors.[7] Thermodynamic and transport properties are composition and temperature dependent, and are evaluated using Chemkin III.[8] Gaseous species diffusivities are computed using mixture averaged transport with effective diffusivities.

2.1 Ethylene Combustion Mechanism

The gas-phase ethylene combustion mechanism was developed by T. Lu and C.K. Law. The mechanism was reduced from a detailed mechanism consisting of 70 species and 463 reactions[9] using the directed relation graph method, sensitivity analysis and computational singular perturbation.[5] The mechanism consists of 19 transported chemical species (H_2, H, O, O_2, OH, H_2O, HO_2, H_2O_2, CH_3, CH_4, CO, CO_2, CH_2O, C_2H_2, C_2H_4, C_2H_6, CH_2CO, C_3H_6, N_2), and 10 quasi-steady-state species. The mechanism was extensively validated for all combustion conditions experienced in the present DNS. These validations consisted of ignition delay, PSR extinction, laminar flame speed, and species concentration profiles in counterflow configurations.[5] The reduced chemical mechanism is tailored to multi-dimensional flow simulation in that it minimizes the number of chemical species that must be transported. In addition, the chemical stiffness is minimized allowing time-step sizes that are limited by acoustics and not by fast chemical scales. The quasi-steady-state species concentrations are computed without the need of nonlinear iteration, which im-

proves computational stability and efficiency. The reduction strategy employed enables DNS with complex chemistry representing increasingly complex hydrocarbon fuels, e.g. in this case ethylene.

2.2 Soot Model

The soot model is based on that of Leung and Lindstedt,[10] which has been used extensively in simulations of turbulent sooting flames. This model is a semi-empirical, four-step model consisting of nucleation, growth, oxidation, and coagulation. The nucleation and growth steps are written in terms of the C_2H_2 concentration. Soot oxidation occurs in a global reaction involving the O_2 concentration, with effects of oxidation via species such as OH and O partially built-in to the rate. While more complex soot chemistry models are available, such as the HACA mechanism,[11] the present mechanism has been widely and successfully used in nonpremixed combustion and is considered adequate for the present purposes in which soot is introduced to DNS.

The soot particle size distribution (PSD) is modelled using the method of moments, in which the first three mass-moments of the PSD are transported. The derivation of the moment transport equations results in fractional moments in the chemical source terms that are closed using an assumed-shape lognormal distribution.[12] This assumption was compared with quadrature closures[13] using four and six moments with excellent agreement. The soot model is fully integrated into the gas-phase mechanism by accounting for mass and energy transfer between the gas and soot phases. Soot particles are small enough that they do not impact the fluid momentum, and are convected with the flow. Soot diffusion is assumed to occur only via thermophoresis as given by

$$j_{Mr} = -0.554 M_r \frac{\nu}{T} \nabla T, \tag{1}$$

where M_r is the r^{th} soot moment, T is temperature, and ν is kinematic viscosity, and j is the diffusion flux. Soot particles have a high molecular weight, and Brownian diffusion is insignificant.

The optically thin radiation model was used, although radiative effects are very small for the domain size and run timescale used.

2.3 Initial Conditions and Configuration

The DNS consists of a temporally evolving, nonpremixed ethylene slot jet. A slab of fuel in the domain center is surrounded by oxidizer. The fuel slab extends to the full range of the stream-wise and span-wise directions, which are periodic. The cross-stream boundary conditions are open, with non-reflecting outflow boundary conditions.[14] The mean flow is one-dimensional in the cross-stream direction, and occurs at nearly constant pressure. This configuration is ideal in that it maximizes the residence time of the fluid in the domain, and provides two homogeneous flow directions for flow statistics.

Table 1: Temporal ethylene jet simulation parameters.

H (mm)	1.8	L_x/H	16	τ_{jet}	0.022
ΔU (m/s)	82	L_y/H	11	τ_{run}/τ_{jet}	50
Re_{jet}	3700	L_z/H	6	# Cells (millions)	228
$u'/\Delta U$ (init)	4%	Δx (μm)	30	Sim. Cost (million cphu)	1.5
H/L_{11} (init)	3	δ_ξ (mm)	0.8		

Parameters used in the simulation are presented in Table 1. The configuration was designed to balance competing costs associated with grid resolution (number of grid cells), total computational run time (maximize the soot reaction time), domain size (maximize Reynolds number and turbulence-flame interactions), and minimize flame extinction. The fuel core width, H, is 1.8 mm, and the difference in velocity streams, ΔU is 82 m/s, giving a jet Reynolds number of 3700. The simulation was run for 50 jet times, τ_j defined by the jet height and velocity difference. The size of the domain is 16H x 11H x 6H in the stream-wise, cross-stream, and span-wise directions, respectively. A grid size of 30 μm was used in each direction, giving a total of 228 million computational grid cells. The simulation is well-resolved for the flow and chemical state fields, with a minimum of 10 grid points across the thinnest radical species structures (e.g. a peak in the profile of a cross-stream cut). The soot fields are less well-resolved with most of the thin structures containing at least five points.

The fuel core velocity is perturbed with three-dimensional isotropic, homogeneous turbulence intended to trip instabilities in the shear layers between the fuel and the oxidizer streams. The turbulence was initialized with $u'/\Delta U = 4\%$, and $H/L_{11} = 3$, where $u'/\Delta U$ is the turbulence intensity and L_{11} is the integral scale.

The flow field composition was initialized by specifying the stream compositions given in Table 2. The stoichiometric mixture fraction is 0.25. The stream composition was varied by moving nitrogen from the oxidizer stream to the fuel stream, hence maintaining a constant adiabatic flame temperature. The mixture fraction varies between zero in the oxidizer stream and one in the fuel stream, with a hyperbolic transition between the streams. A one-dimensional steady laminar flamelet solution was computed with a composition and temperature dependent scalar dissipation rate profile matching the mixture fraction profile in the domain.[5] The transition width corresponds to 50% of the value at extinction. The stream temperatures were both preheated to 550 K. Preheating serves to make the flame more robust towards extinction, and reduced the density ratio between the burned and unburnt mixtures from 8 (with streams at 300 K) to 4.6. The increased ξ_{st} of 0.25, compared to 0.064 for air, also increased the steady extinction scalar dissipation rate. The lower density ratio and more robust flame allowed a greater degree of flame-turbulence interaction than otherwise possible under the time and spatial resolution constraints of the DNS.

Table 2: Stream composition and temperature.

Fuel $\xi = 1$	X_{C2H4}	0.2546
	X_{N2}	0.7454
Oxidizer $\xi = 0$	X_{O2}	0.2641
	X_{N2}	0.7359

Simulations were performed on the Redstorm supercomputer at Sandia National Laboratories. The simulation was run on approximately 8000 processors with a cost of 1.5 million cpuh.

3 RESULTS

3.1 Overview

Figure 1 shows contour plots of temperature and soot mass fraction at $t = 50\tau_j$. On the right are spanwise cuts corresponding to a plane in the streamwise direction with the initial fuel velocity moving to the right. On the left are axial cuts. As the simulation progresses in time, the turbulent shear layers develop and the jet spreads outwards in the cross-stream direction. The flame location also spreads outwards as expansion associated with combustion pushes fluid out of the domain. This figure illustrates the flow configuration and global flame characteristics. There is very little flame extinction occurring, although the flame is highly strained in the so-called braid regions between large-scale vortex structures. A key observation is the difference in the small scale structure of the temperature and soot field. The temperature field is much more diffuse than the soot mass fraction field. All of the soot moments are similar in appearance to the soot mass fraction ($M_1 = \rho Y_{soot}$). The soot diffusivity occurs only via thermophoresis and results in very thin structures. Soot is formed and grows on the fuel-rich side of the flame surface. Turbulent convection acts to essentially stip off the soot into the fuel-rich core where, as soot is mixed with the fuel core, temperature is reduced, and soot reactions become frozen, leaving the soot to be convected and strained with the turbulence.

3.1.1 Scalar dissipation rate

While the Reynolds number of the present flow is moderate, it is in the range of values studied in nonreacting experiments.[15] Figure 2 shows the probability density function (PDF) of $\log_{10}\chi$ at $t = 50\tau_j$. The data are shown on linear and log scales. The data have been normalized to give a mean and standard deviation of zero and one, respectively. The data are conditioned on the mixture fraction taking values between 0.02 and 0.98 to minimize possible bias associated with the pure streams. The DNS data are shown as symbols and a Gaussian distribution (in $\log_{10}\chi$) is shown as the solid line (with the

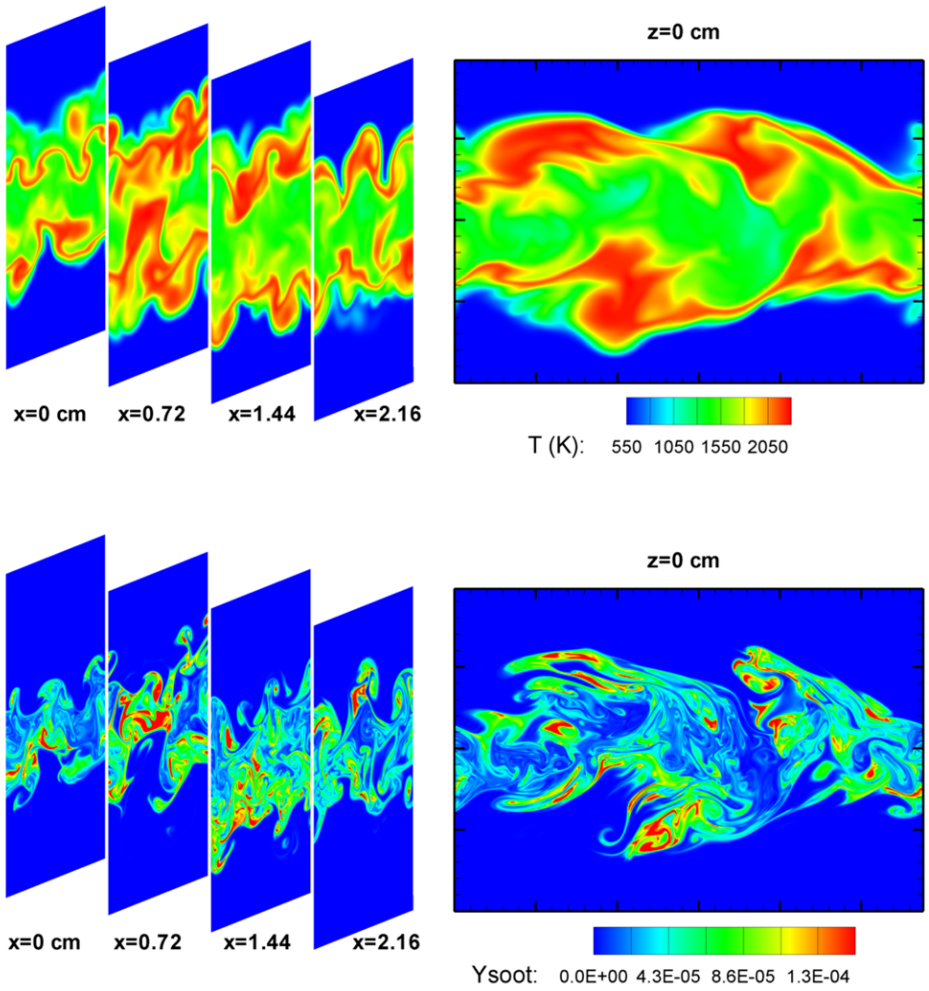

Figure 1: Isoontours of temperature (top) and Y_{soot} (bottom) at $t = 50\tau_j$. The peak Y_{soot} is off scale at 4.5×10^{-4}, located at x=0.72 cm in the center region.

same first two moments as the DNS data). We can see that the DNS data are very nearly lognormal, with a slight negative skewness. These results are in agreement with those previously reported experimentally[15] and in DNS of a similar configuration in an extinction-reignition study of CO-H_2 fuel.[16]

3.2 Conditional Means and Scatter

The combustion and flow characteristics are quantified in Figure 3. This figure shows scatter data from the DNS at $t = 50\tau_j$, as well as the conditional (on mixture fraction) mean and conditional standard deviation as a function of mixture fraction. The mixture fraction computed and used throughout uses the definition of Bilger.[17] The figure shows

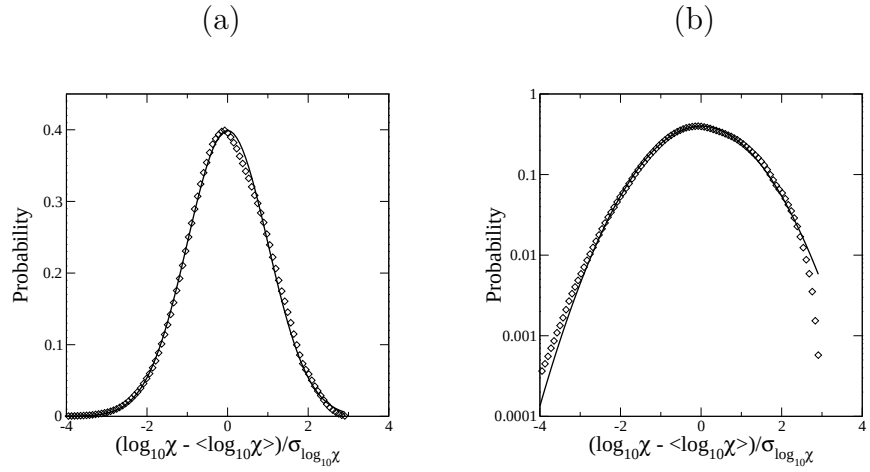

Figure 2: Centered and normalized probability density function of $\log_{10}\chi$ at $t = 50\tau_j$ on linear (a) and log (b) scales. Symbols are data conditioned on $0.02 < \xi < 0.98$. Solid lines are Gaussian distribution with the same first two moments as the DNS data.

temperature, scalar dissipation rate, OH mass fraction (indicative of the flame zone and reactivity) and acetylene (the soot precursor) mass fraction. At $t = 50\tau_j$, the fuel core has mixed out somewhat and the data extends to mixture fractions just below 0.8. The temperature peak occurs just rich of $\xi_{st} = 0.25$, whereas the Y_{OH} peak is lean of this value. This behavior is consistent with the 1D laminar flame solutions. Note that the acetylene concentration peaks at approximately $\xi = 0.5$, which approximately corresponds to the peak in χ. This will have an adverse effect on the concentration of soot obtained in the simulation as a higher χ corresponds to a lower residence time for reaction. The temperature and mass fraction plots show a strong state relationship between the given variable and the mixture fraction. This is indicated by the standard deviation taking values about an order of magnitude lower than the conditional mean. Consistent with experimental observations, the standard deviation of the scalar dissipation rate is seen to be higher than the conditional mean value.[18] Though partially obscured by the logarithmic scale, the conditional mean χ shows a dip around the stoichiometric point. This has been previously observed experimentally,[19] and is consistent with effects of expansion and increased kinematic viscosity (reduced Re) in the flame zone.

At earlier times, the results are qualitatively similar to those at the present time, with the exception that some flame extinction appears in the scatter plots of temperature and OH mass fraction as points significantly below the conditional mean. The conditional mean does not appear to be affected by extinction, however, as the extent of the flame extinction is rather small.

Figure 4 shows scatter data and conditional means and standard deviations of the soot moments (left plots) and the net chemical source terms of the soot moments (right plots). The soot species exhibit distinct behavior from the gaseous species. Note that the

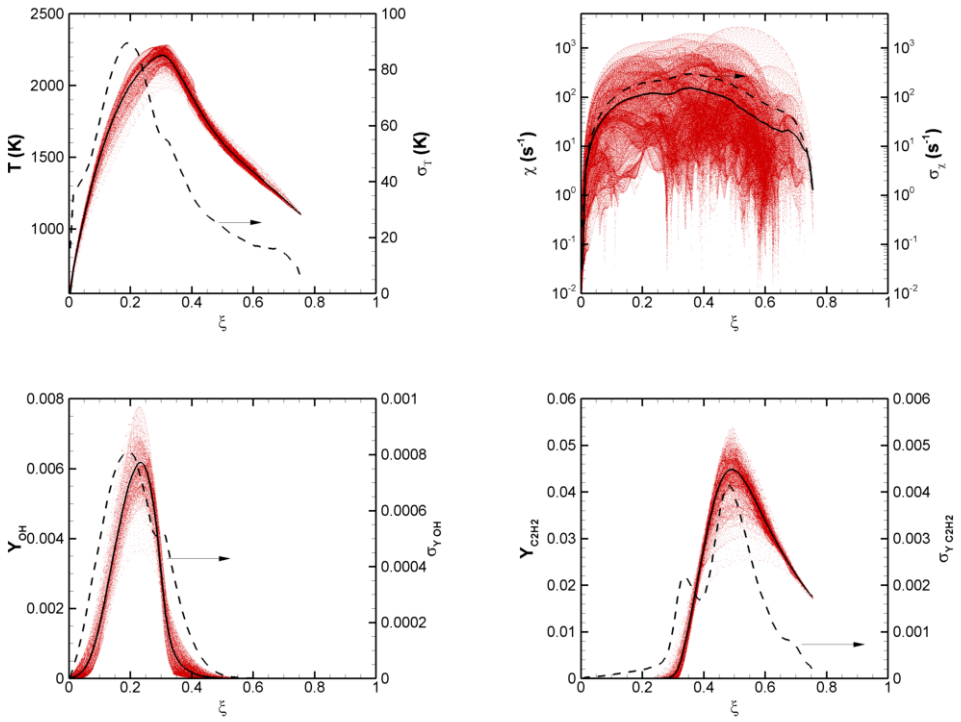

Figure 3: Scatter plots of combustion and flow quantities with conditional means and conditional standard deviations at $t = 50\tau_j$.

conditional scatter in the soot moments is much wider. Hence, the standard deviation of the moments being of the same order of magnitude as the conditional mean. This is in contrast with the gaseous species, where the standard deviation is an order of magnitude lower. It is widely known that soot moments do not have a simple state relationship with mixture fraction. Here, we observe the same result, which is the source of great difficulty in modelling turbulent sooting flames. In previous, two-dimensional DNS, this was shown to be due to the combined effects of unsteady soot growth and strong differential diffusion in the mixture fraction coordinate.[5] This can be seen by comparing the soot moments to their respective reaction rates. The nucleation rate depends only on gaseous species and has similar characteristics, e.g. a relatively low σ. The rates for the second and third moments, while fixed in the mixture fraction coordinate, show much more scatter, consistent with their dependence upon the soot moments. Note the crossover from negative to positive reaction occurs at the ξ_{st} as the soot goes from being consumed in oxidizing regions, to formed in growth regions as the mixture fraction is increased.

The soot moments span the full range of mixture fraction domain fuel-rich of ξ_{st}, whereas the soot rates drop to zero at about $\xi = 0.6$. The only possible mechanism for this is differential diffusion between the soot and mixture fraction, which is the major subject of this paper. This behavior is somewhat masked at $t = 50\tau_j$ since the maximum

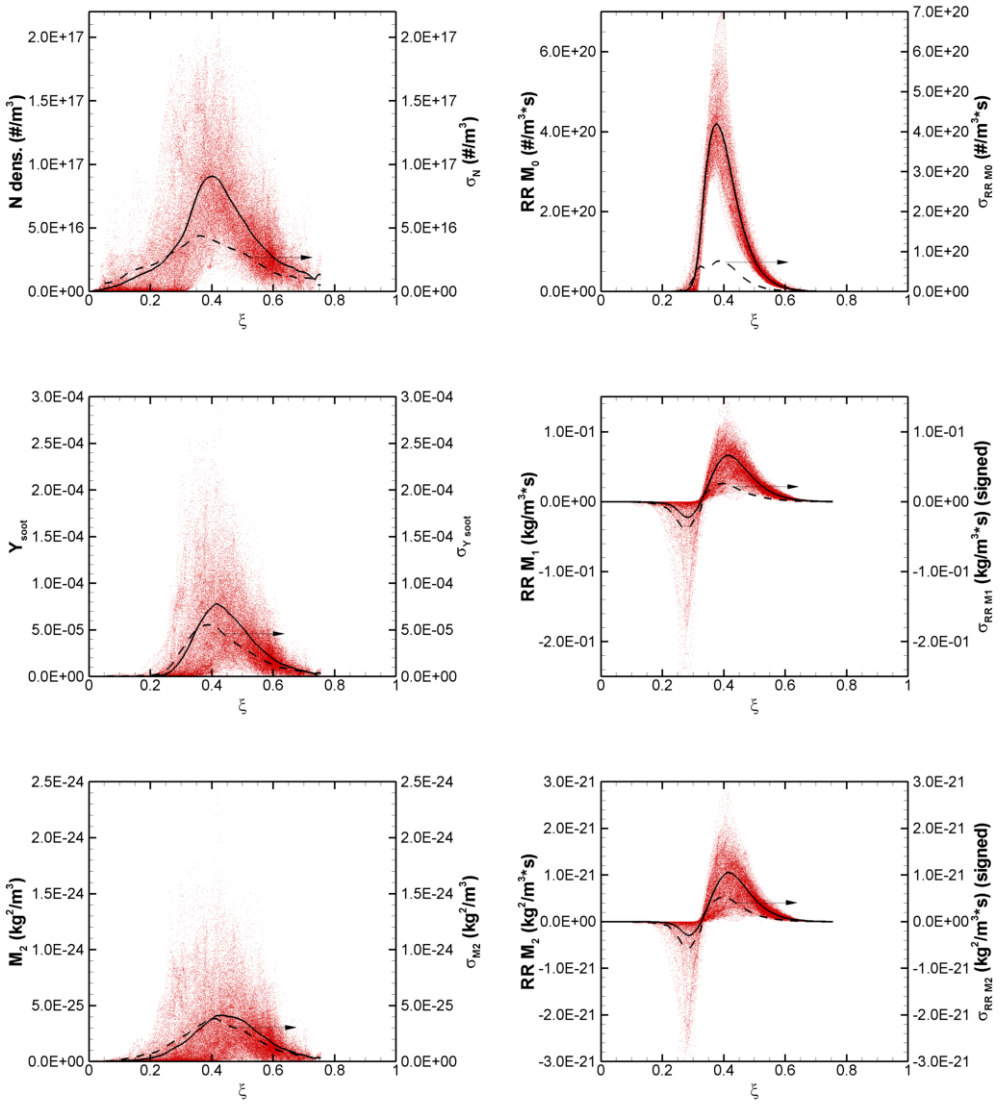

Figure 4: Scatter plots of soot quantities with conditional means and conditional standard deviations at $t = 50\tau_j$.

mixture fraction is below unity. Moreover, due to nitrogen dilution in the fuel core, $\xi_{st} = 0.25$ is much higher than in systems with combustion between pure ethylene and air $\xi_{st} = 0.064$. These two effects render the relative motion between the soot and mixture fraction somewhat obscured, but the picture was obvious in the two-dimensional simulation.[5] In the present simulation, at $t = 25\tau_j$, the peak mixture fraction is near unity and the soot moments extend to this upper bound, whereas the soot rates are limited to the regions of mixture fraction shown in Fig. 4.

On the lean side of ξ_{st}, the second two moments are observed to be practically zero due

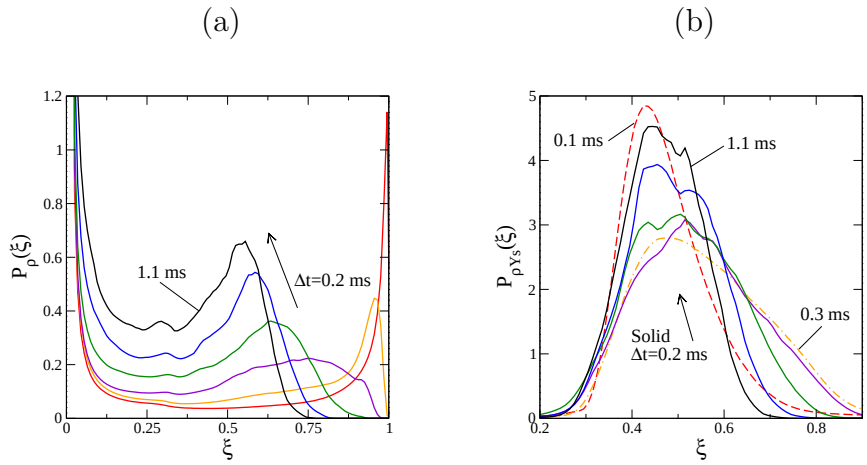

Figure 5: Density (a) and soot mass density weighted (b) probability density functions of mixture fraction at evenly spaced times.

to the oxidation barrier presented by the flame. The number density (M_0) experiences no such barrier since its only sink is coagulation. For M_0, we can see the extent to which differential diffusion between soot and mixture fraction results in soot transported to lean regions. It is possible, that, were the soot mass fraction high enough that oxidation could not fully consume the soot as it is transported past a flame region, substantial quantities of soot could appear fuel-lean of ξ_{st}. This process of soot-flame breakthrough, or at least, soot-ξ_{st} breakthrough in the even of flame quenching, may be important in describing soot emissions. In large-scale fires, a substantial quantity of soot is observed to escape the flames where smoke emission occurs along with radiative shielding.[20] Modelling this process is important for performing predictive simulations of heat transfer in and around fires.

3.3 Mixture Fraction Probability Density Functions and Soot Motion

The motion of the soot in the mixture fraction coordinate is important since this affects the soot concentrations through chemical reactivity, as well as the temperature of the soot, which directly affects radiative emission rates. Figure 5 shows density-weighted (Favre), plot (a), and soot mass density-weighted, plot (b), probability density functions of mixture fraction. Plot (a) is the fraction of mass per unit mixture fraction at the given mixture fraction, while plot (b) is the fraction of the total soot mass per unit mixture fraction at the given mixture fraction. Plot (a) has the form of a β-PDF. At early times, the mixture fraction is partitioned mainly between pure fuel and oxidizer (mostly oxidizer). As time progresses, the fuel stream is mixed out and the upper bound moves towards leaner mixture fraction.

Plot (b) is more interesting; it has a more Gaussian shape, but with a noticeable positive skewness (a tail towards the right). As time evolves, the probability density

function first widens, then contracts. This is explained by two competing effects:

1. Differential diffusion between soot and the mixture fraction, as evidenced by the soot locality outside of the mixture fraction bounds of the soot reaction rates. This differential diffusion occurs due to the dynamics between mixing of soot and isocontours of mixture fraction.

2. As air and fuel mix together, the fuel core is diluted and the upper bound of mixture fraction decreases in time.

Hence, while differential diffusion of soot and mixture fraction tends to spread soot in the mixture fraction coordinate, the upper bound on the mixture fraction is becoming smaller as gas mixing occurs. Time in the present simulation is the analogue of axial position in a nonpremixed jet flame. If the present simulation were continued to longer time, we would expect the peak mixture fraction to approach the oxidizer stream. The soot would be squeezed towards the flame zone until oxidation (and possibly some emission) occurs.

Soot is essentially convected with the fluid, and the rate of motion of isocontours of mixture fraction relative to fluid convection gives the motion of soot with respect to mixture fraction. This motion can be of either positive or negative sign. This was previously demonstrated in two-dimensional simulation[5] by examining the so-called flame displacement velocity v_ξ, and is elaborated on below. In the two-dimensional DNS, the peak mixture fraction did not decrease substantially below unity, and the bulk mixing of the fuel zone was not observed.

Figure 6 highlights the motion and width of $P_{\rho Y_s}$ in Fig. 5. Here we consider the cumulative value of $P_{\rho Y_s}$, denoted simply F. The solid line in Fig. 6 is the value of $F(\xi = 0.5)$ and is the fraction of the total soot mass below a mixture fraction of 0.5. This value starts at over 90% and decreases to below 50% as the soot is transported towards richer ξ. The curve then reaches its minimum point just above 40% and increases to approximately 70% as the fuel is mixed out and the peak mixture fraction decreases. The dashed curve shows the motion of $P_{\rho Y_s}$, as it represents the location in ξ of the median soot mass. This curve is qualitatively the inverse of $F(\xi = 0.5)$ and shows that the peak starts lean at a mixture fraction of about $\xi = 0.4$, which is where the conditional mean of the reaction rate of the number density peaks (and just lean of the peak in the conditional mean of the soot precursor acetylene). The mixture fraction at $F(\xi) = 0.5$ then increases in time to $\xi \approx 0.53$, where it peaks at about the same time as the minimum in $F(\xi = 0.5)$, after which it decreases monotonically to $\xi \approx 0.45$.

3.4 Mixture Fraction Dynamics and Soot-Flame Diffusion

Since soot is essentially convected with the fluid (and diffused via thermophoresis), the differential diffusion between the soot and mixture fraction can be quantified using the velocity of isocontours of the mixture fraction relative to the convective velocity. This velocity occurs via diffusion of iso-scalar surfaces in the direction normal to the surface,

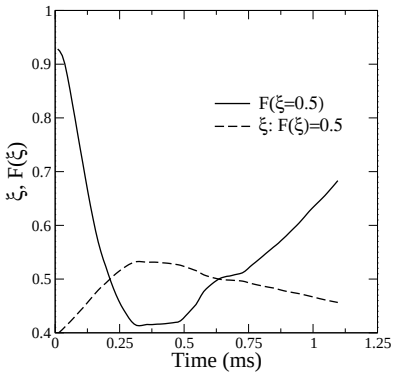

Figure 6: Plot of the soot mass density weighted cumulative probability density function of mixture fraction evaluated at $\xi = 0.5$ (solid). The dashed line shows the mixture fraction location where the same cumulative probability density function has a value of 0.5.

as derived by Gibson.[21] For variable property flow, we have

$$\boldsymbol{v_\xi} = -\frac{\nabla \cdot (\rho D_\xi \nabla \xi)}{\rho |\nabla \xi|} \mathbf{n}. \tag{2}$$

$\boldsymbol{v_\xi}$, the flame displacement velocity, is evaluated at ξ_{st}, where ρ is density, D_ξ is mixture fraction diffusivity obtained assuming a unity Lewis number. $\mathbf{n}$ is the surface normal defined as $\mathbf{n} = \frac{\nabla \xi}{|\nabla \xi|}$, where the normal points towards the fuel stream. Following Echekki and Chen,[22] this velocity can be expanded in terms of the flame normal coordinate into two terms:

$$v_\xi = -D_\xi \nabla \cdot \mathbf{n} - \frac{1}{\rho |\nabla \xi|} \frac{\partial}{\partial \eta} \left(\rho D_\xi \frac{\partial \xi}{\partial \eta} \right) \tag{3}$$

$$= -D_\xi \nabla \cdot \mathbf{n} - \frac{D_\xi}{2} \frac{\partial}{\partial \eta} \ln (\rho^2 D_\xi \chi / 2). \tag{4}$$

Here, η is the flame-normal coordinate in the direction $\mathbf{n}$. The first term is a curvature term where $\nabla \cdot \mathbf{n}$ is the mean surface curvature, and is negative when the center of curvature is in the fuel stream. A negative curvature contributes to v_ξ moving towards the fuel stream, and vice versa. The second term is relative flame motion arising from diffusion in the flame normal direction. This term is rewritten in terms of the scalar dissipation rate in Eq. 4.

In the two-dimensional analysis, it was found that the curvature terms has either sign with a mean near zero, while the normal diffusion term was primarily negative since the flame existed between pure streams at a low mixture fraction, such that a diffusive relaxation of the flame tended to move the flame towards the oxidizer stream. In other words, the second derivative of the mixture fraction in the η coordinate was almost exclusively

positive. Here, ξ_{st} is much higher, hence closer to the inflection point in the ξ profile. This, together with the decreasing upper bound on ξ results in the normal diffusion term taking on both positive and negative values, as shown below.

The terms in Eq. 3 dictate the sign, magnitude and origin of v_ξ, which determines whether soot is locally convected into or away from the flame zone. In the two-dimensional analysis[5] it was found that both terms were of similar magnitude. Here we extend the analysis to three dimensions.

Figure 7 presents the stoichiometric isosurface colored by v_ξ at six time along with grayscale isocontours of the soot mass fraction. Note that the scale varies with time. At early times there is a strong positive correlation between the soot concentration and the magnitude and sign of v_ξ. Regions of positive v_ξ correspond to the flame moving towards the fuel stream relative to convection. In these regions the soot is locally convected towards the flame zone where its temperature is higher and the soot is more reactive. This behavior was observed in two-dimensional. There, the turbulence was decaying, the Reynolds number was smaller and the soot was not strongly convected away from the flame zone. Here, at $23\tau_j$, spanwise rollers associated with the Kelvin-Helmholz shear instability transports the soot away from the flame zone. These strong transport and history effects complicate the analysis. Ideally, a Lagrangian description of the soot would record the full history, especially the reactive history, of the soot. As it is, soot is formed and grown in reactive zones near the flame. Turbulence transports the soot away from the flame where mixing quenches reaction, but soot remains to be strained and diluted. The soot structures persist even as the turbulent energy decays, serving as an example of Gibson's so-called fossil turbulence.[23]

At later times, e.g. $t = 32\tau_j$ there are regions of high v_ξ for which the soot concentration appears to be very small. There are two possible reasons for this. One is simply that the thickness of the colored stoichiometric surface obscures a high concentration of soot beneath it. This occurs, for example, at $t = 32\tau_j$ on the right of the upper flame sheet. More importantly, the flame sheet is wrinkled with a curvature that can rapidly change sign, which, therefore, can change the sign of v_ξ. If this occurs on a timescale that is small compared to the soot reaction timescales, its effect will not be visible.

At $t = 32\tau_j$, mixture fraction contours at 0.15 and 0.35 are also shown. Note that in some regions, soot is absent "far" from the flame, but that these regions, in fact, appear to coincide with the spacing of the mixture fraction contours. That is, the soot is not "far" from the flame in the mixture fraction coordinate where extensive strain rates in the upstream portions of the spanwise rollers separates the mixture fraction isocontours. From Fig. 4, the crossover between production and destruction of $M_1 = \rho Y_s$ occurs at about $\xi = 0.33$.

3.5 The Flame Displacement Velocity and Its Terms

Figure 8 show the marginal probability density functions of v_ξ and its budget at three times corresponding to $5\tau_j$, $23\tau_j$ and $41\tau_j$. These probability density functions show

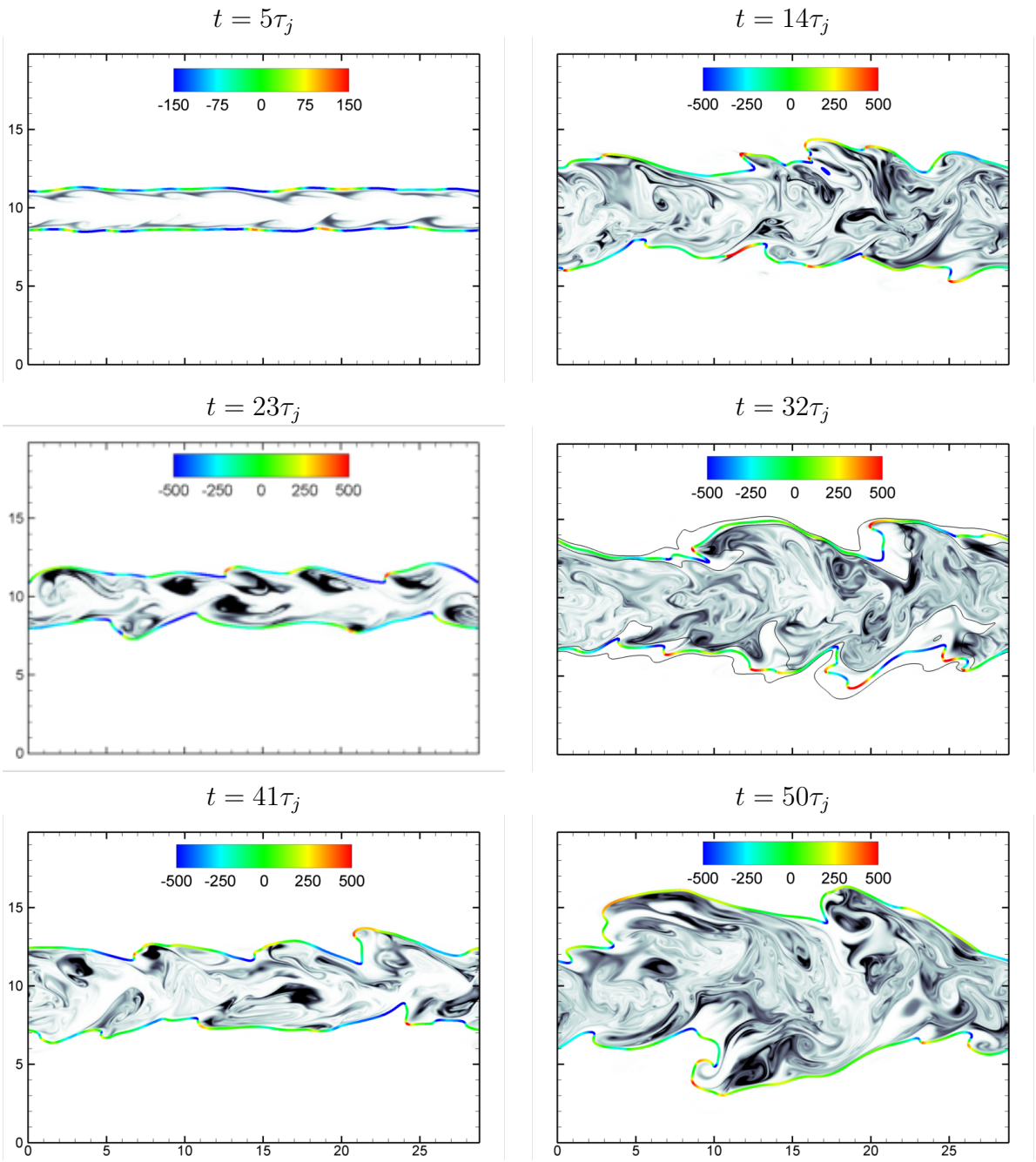

Figure 7: Y_{soot} (grayscale, black is high value) and stoichiometric isosurface colored by v_ξ. The scales vary: with increasing time the peak Y_{soot} scale is 1×10^{-5}, 1×10^{-5}, 4×10^{-5}, 5×10^{-5} 10×10^{-5}, 15×10^{-5}. The length dimension is mm. At $32\tau_j$ two additional mixture fraction isocontours , 0.15 and 0.35 are shown.

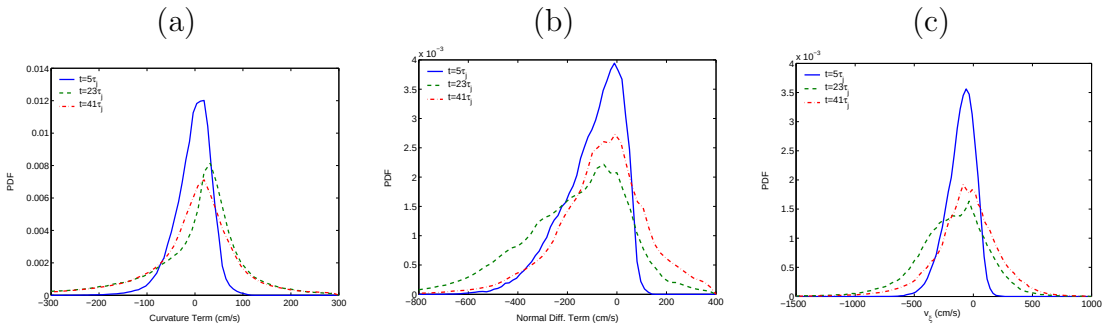

Figure 8: Marginal probability density functions of v_ξ, Eq. 2, and its two terms Eqns. 3 and 4, conditioned on ξ_{st} at three times ($5\tau_j$, $23\tau_j$, $41\tau_j$).

that both terms of v_ξ are of similar magnitude throughout the simulation. As the jet develops in time, the variance of both terms is observed to grow, whereas the peak value is relatively constant (compared to the range). The mean and standard deviation of both terms (not shown) decrease in time to a minimum at around $23\tau_j$, then increase. The mean curvature term decreases from zero to -11 cm/s, then increases to -2 cm/s at $t = 0$, $23\tau_j$, $50\tau_j$, respectively. The normal diffusion term decreases from -100 cm/s to -170 cm/s, then increases to -20 cm/s at the same times. While the mean curvature is nearly zero throughout the simulation, the mean curvature term is slightly negative. This is due to the temperature dependence of D_ξ, and the location of ξ_{st}. When the flame has a negative curvature, χ_{st} tends to be higher than when the flame has a positive curvature. This results in a lower flame temperature, and a lower D_ξ. The χ, curvature (κ) relation at ξ_{st} results from the bias towards extensive strain of $\xi <\approx 0.5$ with negative curvature. The joint PDF of χ_{st} with κ_{st} (not shown) indicates a negative correlation.

The normal diffusion term is observed to have a strong negative skewness. As noted previously, in the absence of curvature, an ideal diffusion flame with $\xi_{st} <\approx 0.5$ will have a positive second derivative for which diffusive relaxation will move the flame towards the oxidizer. This effect is less strong as ξ_{st} increases towards the inflection point (at which time the sign changes and the diffusive relaxation causes flame motion towards the fuel side). This effect is enhanced as the peak mixture fraction decreases due to mixing. As time progresses, a significant portion of the flame exists with a positive normal diffusion term. The effect of the terms on the marginal, stoichiometric probability density function of v_ξ is also shown in the figure. v_ξ is always biased to negative values, as expected due to the practically zero mean of the curvature term and the negative bias of the normal diffusion term. In time, however, this bias is reduced and the fraction of positive v_ξ increases from about 15% to nearly 50%.

This point is important from a modelling perspective because it means that multi-dimensional effects associated with flame curvature, and mixing effects associated with normal diffusion can result in a diffusion flame that moves (relative to convection) in both the fuel and oxidizer directions with nearly equal frequency. Positive v_ξ is the opposite

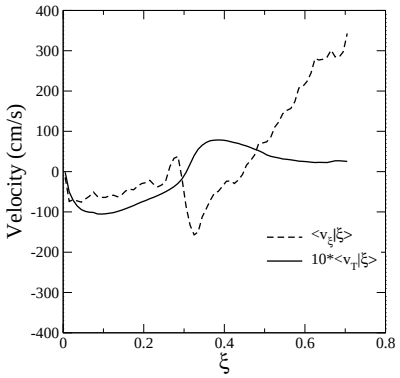

Figure 9: Conditional mean thermophoretic (solid) and flame displacement (dashed) velocities at $t = 50\tau_j$.

of what occurs in canonical opposed jet diffusion flames of similar stream compositions. While these effects may play a small role in the combustion gas dynamics, they are shown to play a strong role in soot formation and radiative processes in the two-dimensional simulations. Here, it is demonstrated that similar flame dynamics are observed in both two- and three-dimensional turbulence.

3.6 Thermophoretic Diffusion Velocity

Figure 9 shows the conditional mean thermophoretic diffusion velocity $< v_T|\xi >$ and flame displacement velocity at $t = 50\tau_j$. Here, $< v_\xi|\xi >$ refers to the velocity at the given mixture fraction, and not the stoichiometric surface, as above. Note that the scale of $< v_T|\xi >$ is a factor ten lower than the scale of $< v_\xi|\xi >$, while the curves are of similar magnitude. Hence, the thermophoretic velocity is much smaller than the differential diffusion velocity between the gas and the soot fields.

4 DISCUSSION

As the first extension of soot formation to turbulent DNS with complex chemistry, several concessions were made. The present soot model does not account for the role of PAH and radical species (such as H) in the nucleation, growth and oxidation processes. Quantitative detailed soot models are the subject of ongoing research. The effect of detailed soot chemistry will impact the location of the soot reactivity within the flame zone and may alter the quantitative soot concentrations. However, the primary results focusing on the flame dynamics and soot-flame interaction with soot transport over the full range of ξ are not expected to be sensitive to the details of the soot model employed.

In order to resolve the time and length scales of the simulation with a fixed computational cost, the simulation time was limited to 1.1 ms. This relatively low time, and the relatively high turbulence experienced by the flame results in lower soot concentrations

($f_{v,peak} = 0.03$), comparable to experimental values in methane flames.[24] In larger-scale configurations (e.g. fires) longer soot residence times for growth and radiative transfer with significantly stronger soot-flame interaction are expected. However, the basic interactions between soot and the flame due to differential transport influenced by the flame dynamics are expected to remain.

5 CONCLUSIONS

Large-scale, three-dimensional DNS of a turbulent ethylene jet flame has been performed with realistic chemistry and transport. The simulation included soot formation using a standard model and represents the first DNS of soot formation in a three-dimensional turbulent flame. Previous analyses from two-dimensional simulation in decaying turbulence were applied in the present three-dimensional jet configuration. While the three-dimensional simulation is substantially more complex than the two-dimensional simulation, the major conclusions of the two-dimensional results are unchanged. Important results from the present simulation are summarized below:

- The turbulent flame yields a lognormal probability density function of scalar dissipation rate with a negative skewness in agreement with nonreacting experimental data and reacting DNS results.
- Motion of soot in the mixture fraction coordinate arises from differential diffusion between soot and mixture fraction, as well as the bulk effect of mixing of the fuel jet core. The location of soot in the mixture fraction coordinate directly influences the temperature and gas composition that the soot experiences, hence its radiative heat transfer and reaction rates.
- To quantify the differential diffusion between the gas and the soot, the diffusive velocity of mixture fraction isocontours relative to convection, v_ξ is computed at the flame surface. A positive value of v_ξ results in motion of the ξ surface towards the fuel stream (and vice versa). The curvature and normal diffusion terms of v_ξ are computed and found to be of similar magnitude and of either sign.
- A substantial portion of the ξ_{st} surface (nearly 50%) has $v_\xi > 0$. In these regions soot is convected towards the flame, which is the opposite of what occurs in canonical opposed jet/flamelet configurations commonly used in modelling.
- The thermophoretic velocity is found to be lower than v_ξ by an order of magnitude over the range of ξ, indicating that thermophoretic effects are small compared to differential diffusion effects between gaseous species and soot.

6 ACKNOWLEDGMENTS

This work was supported by the U. S. Department of Energy, Office of Basic Energy Sciences, Division of Chemical Sciences, Geosciences, and Biosciences. Simulations were

performed at Sandia National Laboratories on the Redstorm supercomputer. Sandia National Laboratories is a multiprogram laboratory operated by Sandia Corporation, a Lockheed Martin Company, for the United States Department of Energy under contract DE-AC04-94-AL85000.

REFERENCES

[1] M. D. Smooke, R. J. Hall, M. B. Colket, J. Fielding, M. B. Long, C. S. McEnally, and L. D. Pfefferle. Investigation of the transition from lightly sooting towards heavily sooting co-flow ethylene diffusion flames. *Combust. Theor. Model.*, 8:593–606, 2004.

[2] C. R. Shaddix, T. C. Williams, L. G. Blevins, and R. W. Schefer. Flame structure of steady and pulsed sooting inverse jet diffusion flames. *Proc. Combust. Inst.*, 30:1501–1508, 2005.

[3] P. E. Desjardin and S. H. Frankel. Two-dimensional large eddy simulation of soot formation in the near-field of a strongly radiating nonpremixed acetylene-air turbulent jet flame. *Combust. Flame*, 119:121–132, 1999.

[4] H. Pitsch, E. Riesmeier, and N. Peters. Unsteady flamelet modelling of soot formation in turbulent diffusion flames. *Combust. Sci. Technol.*, 158:389–406, 2000.

[5] D. O. Lignell, J. H. Chen, P. J. Smith, T. F. Lu, and C. K. Law. The effect of flame structure on soot formation and transport in turbulent nonpremixed flames using direct numerical simulation. *Combust. Flame*, in press, 2007.

[6] C. A. Kennedy, M. H. Carpenter, and R. M. Lewis. Low-storage, explicit runge-kutta schemes for the compressible navier-stokes equations. *Appl. Num. Math.*, 35(3):177–219, 2000.

[7] C. A. Kennedy and M. H. Carpenter. A comparison of several new numerical methods for the simulation of compressible shear layers. *Appl. Num. Math.*, 14(4):397–433, 1994.

[8] R. J. Kee, F. M. Rupley, and J. A. Miller. *Chemkin*. Reaction Design, Inc., San Diego CA, 2000.

[9] Z. Qin, V. V. Lissianski, H. Yang, W. C. Gardiner, S. G. Davis, and H. Wang. Combustion chemistry of propane: a case study of detailed reaction mechanism optimization. *Proc. Combust. Inst.*, 28:1663–1669, 2000.

[10] K. M. Leung and R. P. Lindstedt. A simplified reaction mechanism for soot formation in nonpremixed flames. *Combust. Flame*, 87:289–305, 1991.

[11] J. Appel, H. Bockhorn, and M. Frenklach. Kinetic modelling of soot formation with detailed chemistry and physics: laminar premixed flames of c_2 hydrocarbons. *Combust. Flame*, 121:122–136, 2000.

[12] S. E. Pratsinis. Simultaneous nucleation, condensation, and coagulation in aerosol reactors. *J. Colloid. Interf. Sci.*, 124(2):416–427, 1987.

[13] R. McGraw. Description of aerosol dynamics by the quadrature method of moments. *Aerosol. Sci. Tech.*, 25:255–265, 1997.

[14] J. C. Sutherland and C. A. Kennedy. Improved boundary conditions for viscous reacting compressible flows. *J. Comput. Phys.*, 191:502–524, 2003.

[15] L. K. Su and N. T. Clemens. The structure of fine-scale scalar mixing in gas-phase planar turbulent jets. *J. Fluid Mech.*, 488:1–29, 2003.

[16] E. R. Hawkes, R. Sankaran, J. C. Sutherland, and J. H. Chen. Scalar mixing in direct numerical simulations of temporally-evolving plane jet flames with detailed co/h_2 kinetics. *Proc. Combust. Inst.*, 31:1633–1640, 2007.

[17] R. W. Bilger, S. H. Starner, and R. J. Kee. On reduced mechanisms for methan-air combustion in nonpremixed flames. *Combust. Flame*, 80(2):135–149, 1990.

[18] E. Effelsberg and N. Peters. Scalar dissipation rates in turbulent jets and jet diffusion flames. *Proc. Combust. Inst.*, 22:693–700, 1988.

[19] A. N. Karpetis and Barlow R. S. Measurements of flame orientation and scalar dissipation in turbulent partially premixed methane flames. *Proc. Combust. Inst.*, 30:665–672, 2005.

[20] H. Koseki. Combustion properties of large liquid pool fires. *Fire Technology*, 25:241–255, 1989.

[21] C. H. Gibson. Fine structure of scalar fields mixed by turbulence. i. zero-gradient points and minimal gradient surfaces. *Phys. Fluids*, 11(11):2305–2315, 1968.

[22] T. Echekki and J. H. Chen. Analysis of the contribution of curvature to premixed flame propagation. *Combust. Flame*, 118:308–311, 1999.

[23] C. H. Gibson. Turbulence in the ocean, atmosphere, galaxy, and universe. *Applied Mechanical Review*, 49:299–315, 1996.

[24] A. Beltrame, P. Porshnev, W Merchan-Merchan, A. Saveliev, A. Fridman, and L. A. Kennedy. Soot and no formation in methane-oxygen enriched diffusion flames. *Combust. Flame*, 124:295–310, 2001.